

Augmentation of Generalized Multivariable Grid-Forming Control for Power Converters with Cascaded Controllers

Meng Chen¹, Dao Zhou¹, Ali Tayyebi², Eduardo Prieto-Araujo³, Florian Dörfler², and Frede Blaabjerg¹

¹AAU Energy, Aalborg University, Aalborg, Denmark

²Automatic Control Laboratory, Swiss Federal Institute of Technology (ETH) Zurich, Zurich, Switzerland

³CITCEA-UPC, Technical University of Catalonia, Barcelona, Spain

{mche, zda}@energy.aau.dk, alit@student.ethz.ch, eduardo.prieto-araujo@upc.edu, dorfler@ethz.ch, fbl@et.aau.dk

Abstract—The classic design of grid-forming control strategies for power converters rely on the stringent assumption of the timescale separation between DC and AC states and their corresponding control loops, e.g., AC and DC loops, power and cascaded voltage and current loops, etc. This paper proposes a multi-input multi-output based grid-forming (MIMO-GFM) control for the power converters using a multivariable feedback structure. First, the MIMO-GFM control couples the AC and DC loops by a general multivariable control transfer matrix. Then, the parameters design is transformed into a standard fixed-structure \mathcal{H}_∞ synthesis. By this way, all the loops can be tuned simultaneously and optimally without relying on the assumptions of loop decoupling. Therefore, a superior and robust performance can be achieved. Experimental results verify the proposed method.

Index Terms—multi-input multi-output based grid-forming (MIMO-GFM) control, cascaded controllers, loops coupling, fixed-structure \mathcal{H}_∞ synthesis

I. INTRODUCTION

The design of grid-forming controllers is complicated, as there always are many nested loops to be tuned in order to simultaneously achieve multiple objectives, e.g., stability, power regulation, synchronization, etc [1]. Therefore, several assumptions are usually made in traditional grid-forming control architectures. Firstly, the DC and AC dynamics are supposed to be decoupled [2]. Secondly, it is assumed that the active and reactive powers can be controlled independently [3]. Thirdly, the cascaded voltage and current loops are often neglected due to their large bandwidths compared with the power loops, e.g., in low-power converters [4].

The above assumptions simplify the grid-forming control design to several decoupled single-input single-output (SISO) systems, e.g., DC loop, AC power loops, and cascaded loops, which can be separately designed and tuned. When focusing on the AC dynamics, an ideal DC source is typically used in most prevalent grid-forming controllers, e.g., droop control, virtual synchronous generator (VSG), etc [1], [2]. With respect to the cascaded controllers, the symmetrical optimum criterion and modulus optimum criterion can be used [5], [6]. Thereafter, predefined p - f and q - V relationships are usually used

to construct the active and reactive power loops, respectively, where typical designs are based on the classic control methods, e.g., root-locus and frequency analysis [2], [7].

Nevertheless, the aforementioned assumptions can not provide a superior and robust performance. On one hand, the loops decoupling is not always reasonable due to the fact that the low switching frequency of a high-power converter limits the bandwidths of the cascaded controllers. In this context, a complete model has to be used [5], [6]. On the other hand, these simplifications limit the bandwidths of the power loops [8] and they also discard the useful information in the coupling terms, which have proved to be favorable in [9]–[12], especially regarding the DC dynamics. Moreover, the manual parameter tuning based on the classic control methods is cumbersome and inconvenient when coping with multiple parameters.

Recently, the $\mathcal{H}_2/\mathcal{H}_\infty$ synthesis begins to be used in the grid-forming controller and the VSC-HVDC link design, which, compared with the aforementioned methods, can achieve a multi-objective optimization by simultaneously tuning all the loops [13]–[19]. In [18], the power loops and inner voltage loop are considered. However, the important DC dynamics are neglected, which influences the performance of the controllers. A multi-input multi-output based grid-forming (MIMO-GFM) control is proposed in [19] by coupling the DC loop and the AC power loops, which shows a superior and robust performance. Nevertheless, the cascaded controllers are not considered. Therefore, this paper extends the work of [19] by including the cascaded controllers into the fixed-structure \mathcal{H}_∞ synthesis. In this way, the following advantages can be achieved.

- 1) The assumptions of bandwidths (or timescales) separation among different loops, e.g., cascaded voltage and current loops, and power loops, can be removed.
- 2) The assumptions of loops decoupling, e.g., active and reactive power loops, and DC loop, can be removed.
- 3) The parameters can be tuned simultaneously and automatically in order to obtain an optimal performance.

We experimentally validate the superior performance of our

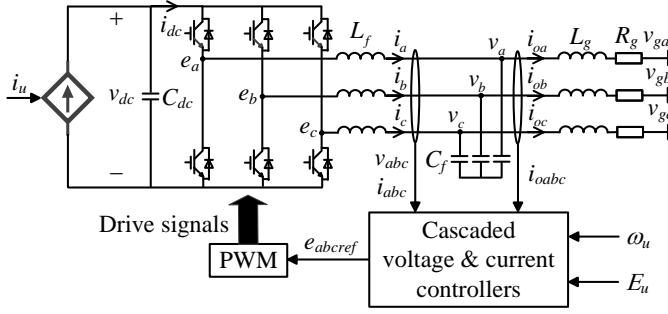


Fig. 1. DC-AC power converter configuration with low-level cascaded controllers that process the references i_u , ω_u , and E_u provided by a high-level grid-forming control strategy.

design in comparison to a standard VSG control with nested, time-scale separated, and decoupled loops.

The remainder of paper is organized as follows. The model of the MIMO-GFM converter with cascaded controllers is built in Section II. In Section III, the formulation of the fixed-structure \mathcal{H}_∞ synthesis for the MIMO-GFM converter with cascaded controllers are given. In Section IV, experimental results are shown, and finally, conclusions are given in Section V.

II. MODELING OF MIMO-GFM WITH CASCADED CONTROLLERS

Fig. 1 shows the topology of the grid-forming converter controlled with cascaded controllers, where the power stage consists of a three-phase converter and an LC filter with L_f and C_f being its inductor and capacitor. In the MIMO-GFM converter, the DC source is represented by a controlled current source i_u in order to consider the dynamics of the DC capacitor C_{dc} and free the assumption of an ideal DC source. Moreover, ω_u and E_u are the inputs of frequency and voltage to achieve the ability of grid-forming, which are used as the references of the cascaded controllers. Therefore, a MIMO-GFM controller should provide three inputs, i.e., i_u , ω_u , and E_u for both the DC and AC loops.

The power stage model of the MIMO-GFM converter of Fig. 1, in the ω_u -defined d - q frame can be summarized as

$$\dot{i}_d = \frac{\omega_b}{L_f} e_d - \frac{\omega_b}{L_f} v_d + \omega_b \omega_u i_q \quad (1)$$

$$\dot{i}_q = \frac{\omega_b}{L_f} e_q - \frac{\omega_b}{L_f} v_q - \omega_b \omega_u i_d \quad (2)$$

$$\dot{v}_d = \frac{\omega_b}{C_f} i_d - \frac{\omega_b}{C_f} i_{od} + \omega_b \omega_u v_q \quad (3)$$

$$\dot{v}_q = \frac{\omega_b}{C_f} i_q - \frac{\omega_b}{C_f} i_{oq} - \omega_b \omega_u v_d \quad (4)$$

$$\dot{i}_{od} = \frac{\omega_b}{L_g} v_d - \frac{\omega_b}{L_g} V_g \cos \delta - \frac{\omega_b R_g}{L_g} i_{od} + \omega_b \omega_u i_{oq} \quad (5)$$

$$\dot{i}_{oq} = \frac{\omega_b}{L_g} v_q + \frac{\omega_b}{L_g} V_g \sin \delta - \frac{\omega_b R_g}{L_g} i_{oq} - \omega_b \omega_u i_{od} \quad (6)$$

$$\dot{v}_{dc} = \frac{\omega_b}{C_{dc}} i_u - \frac{\omega_b (e_d i_d + e_q i_q)}{C_{dc} v_{dc}} \quad (7)$$

where e_d and e_q are the output voltages, v_d and v_q are the capacitor voltages, i_d and i_q are the inductor currents of the filter, i_{od} and i_{oq} are output currents, v_{dc} is the DC voltage, V_g is grid voltage magnitude, ω_b is the base value of the angular frequency, δ is the angle difference between the MIMO-GFM controller frame and the power grid frame, which is defined as

$$\dot{\delta} = \omega_b \omega_u - \omega_b \omega_g \quad (8)$$

where ω_g is the grid frequency. The dynamics of v_{dc} in (7) shows the natural coupling between AC and DC sides.

The cascaded controllers use PI controllers with decoupling and feedforward terms, whose control commands are

$$i_{dref} = k_{pv}(E_u - v_d) + k_{iv} \int_0^t (E_u - v_d) d\tau - C_f v_q + k_{ffi} i_{od} \quad (9)$$

$$i_{qref} = k_{pv}(-v_q) + k_{iv} \int_0^t (-v_q) d\tau + C_f v_d + k_{ffi} i_{oq} \quad (10)$$

$$e_{dref} = k_{pi}(i_{dref} - i_d) + k_{ii} \int_0^t (i_{dref} - i_d) d\tau - L_f i_q + k_{ffv} v_d \quad (11)$$

$$e_{qref} = k_{pi}(i_{qref} - i_q) + k_{ii} \int_0^t (i_{qref} - i_q) d\tau + L_f i_d + k_{ffv} v_q \quad (12)$$

where k_{pv} and k_{iv} are gains of voltage PI controllers, k_{pi} and k_{ii} are gains of current PI controllers, k_{ffi} and k_{ffv} are gains of feedforward terms of voltage and current controllers, i_{dref} and i_{qref} are current references, e_{dref} and e_{qref} are the references of the converter voltages.

The impact of PWM and sampling delay can be estimated by [5], [6]

$$\dot{e}_d = \frac{1}{1.5T_{sw}} e_{dref} - \frac{1}{1.5T_{sw}} e_d \quad (13)$$

$$\dot{e}_q = \frac{1}{1.5T_{sw}} e_{qref} - \frac{1}{1.5T_{sw}} e_q \quad (14)$$

where T_{sw} is the switching cycle. Therefore, the bandwidths of the cascaded controllers is strongly limited by the employed switching frequency. As a result, the cascaded controllers can not be neglected as usual for the power converters with low switching frequencies [6].

For the grid-forming converter, typically five output quantities are considered, i.e., the active and reactive power p and q , magnitude of the terminal voltage V , the frequency assigned by the grid-forming control ω_u , as well as v_{dc} , where p , q , V are expressed by the state variables as follows:

$$p = v_d i_{od} + v_q i_{oq} \quad (15)$$

$$q = -v_d i_{oq} + v_q i_{od} \quad (16)$$

$$V = \sqrt{v_d^2 + v_q^2} \quad (17)$$

According to (1)-(17), the MIMO open-loop equivalent model of the grid-forming converter with cascaded controllers is shown in Fig. 2, which represents a three-input five-output system where the grid voltage is treated as a disturbance.

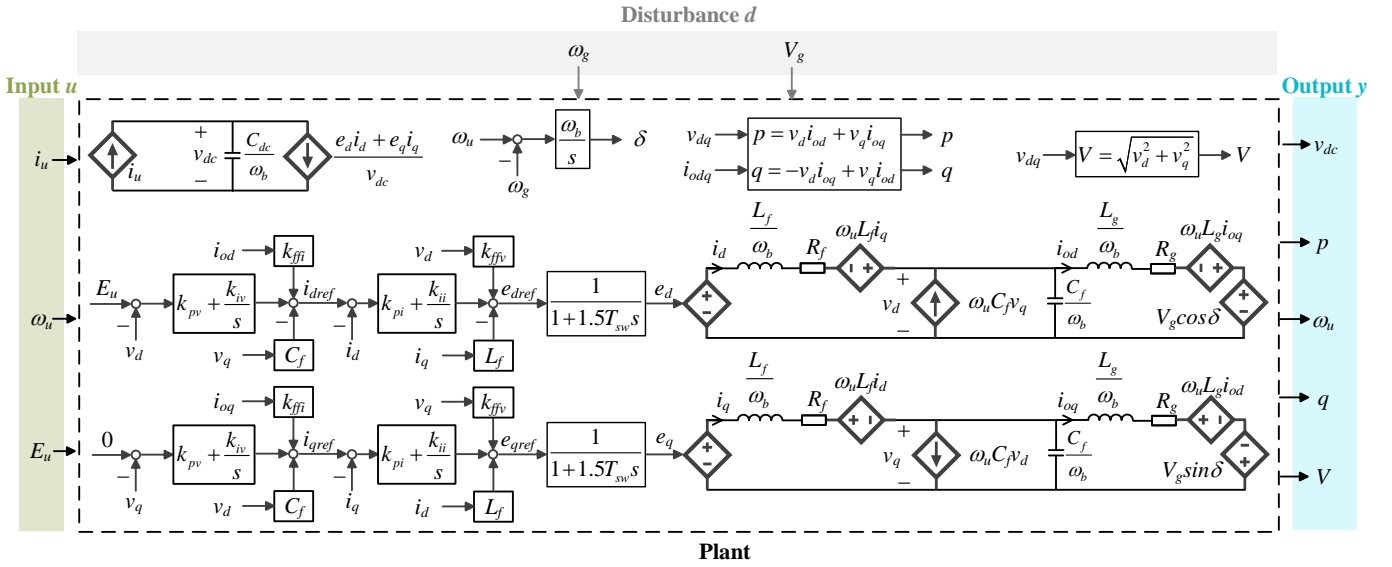


Fig. 2. MIMO open-loop equivalent circuit of grid-forming converter with cascaded controllers in d - q frame.

For notational convenience, we define the vectors:

$$\mathbf{x} = [e_d \ e_q \ i_d \ i_q \ v_d \ v_q \ i_{od} \ i_{oq} \ v_{dc} \ \delta]^T \quad (18)$$

$$\mathbf{e}_{ref} = [e_{dref} \ e_{qref}]^T, \quad \mathbf{u} = [i_u \ \omega_u \ E_u]^T \quad (19)$$

$$\mathbf{y} = [v_{dc} \ p \ \omega_u \ q \ V]^T \quad (20)$$

$$\mathbf{d} = [\omega_g \ V_g]^T, \quad (21)$$

where \mathbf{x} is the state vector of the power stage, \mathbf{u} is the control vector, \mathbf{y} is the output vector, and \mathbf{d} is the disturbance vector. Thereafter, the equivalent circuit of Fig. 2 can be abstracted as a compact open-loop model as in Fig. 3. Similar to the control synthesis in [19], this open-loop model is closed by the multivariable MIMO-GFM feedback control as illustrated in Fig. 4.

$$\mathbf{u}_0 = [i_0 \ \omega_0 \ E_0]^T \quad (22)$$

$$\mathbf{Y}_{ref} = [V_{dcref} \ P_{ref} \ \omega_g \ Q_{ref} \ V_{ref}]^T \quad (23)$$

$$\Phi = (\phi_{ij})_{3 \times 5}, \quad (24)$$

where \mathbf{u}_0 is the vector of set-points for \mathbf{u} , \mathbf{Y}_{ref} is the vector of references for \mathbf{y} . In addition, \mathbf{e} is the vector of error signals. We notice that $\Phi = \Phi(s)$ is the 3×5 control transfer matrix. The performance of the grid-forming controller is therefore grounded on the choices of Φ , where a reasonable choice is

$$\Phi = \begin{bmatrix} k_{pdc} + k_{idc}/s & k_{12} & 0 & k_{14} & k_{15} \\ k_{21} & D_p k_{22}/(s + k_{22}) & 0 & k_{24} & k_{24}/D_q \\ k_{31} & k_{32} & 0 & k_{34}/s & k_{34}/D_q \end{bmatrix} \quad (25)$$

where D_p and D_q are droop coefficients to achieve a proper power sharing in the case of multiple MIMO-GFM converters, the PI controller of ϕ_{11} guarantees a zero-error of the DC voltage in the steady-state, the low-pass filter of ϕ_{22} provides inertia characteristics like in a synchronous generator, and the

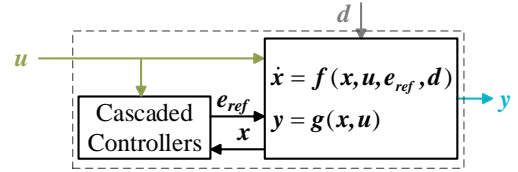


Fig. 3. Compact MIMO open loop equivalent model of grid-forming converter with cascaded controllers - see Fig. 2 for details.

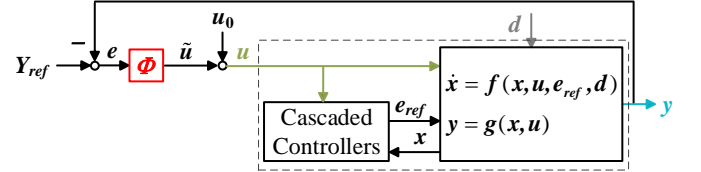


Fig. 4. Compact MIMO close loop feedback control of grid-forming converter with cascaded controllers.

third column with zeros avoids the dependence on ω_g and, therefore, realize a complete phase-locked-loop-free (PLL-free) system. It is noted that Φ in (25) couples all the DC and AC power loops in a single monolithic controller.

III. \mathcal{H}_∞ SYNTHESIS OF MIMO-GFM WITH CASCADED CONTROLLERS

As shown in (25), unlike perceiving the grid-forming converter as several decoupled SISO systems [2]–[4], the MIMO-GFM controller accounts for the natural system couplings and thus highly improves the performance of the power converter by assigning simple proportional controllers rather than high-order terms (e.g., damping terms based on PLL or high-order filters). Thereafter, another problem is how to choose the parameters for an optimal performance. Classic methods are manual tuning based on root-locus or frequency analysis,

which may be very inconvenient when simultaneously selecting multiple parameters. Therefore, the bandwidths of the cascaded voltage and current loops as well as power loops are usually chosen in different timescales. Then they are designed separately, which, nevertheless, has several shortages. First, the loops' decoupling between DC and AC sides is not true for the MIMO-GFM controller. Second, the bandwidths of the cascaded voltage and current loops may not be high enough for a high-power converter with low switching frequency (e.g., 2 kHz). Third, the performance may be limited in order to keep the bandwidths separation. To cope with these issues, in what follows we transform the parameters design of the MIMO-GFM controller with cascaded controllers into an \mathcal{H}_∞ synthesis. As a result, all the nested loops are simultaneously tuned to obtain an optimal performance.

To this end, the tuned parameters in both the control transfer matrix Φ and cascaded controllers should be separated as shown in Fig. 5. Two intermediate vectors \hat{y} and \hat{u} are introduced and have the following relationship

$$\begin{aligned} \hat{u} = & \text{diag}(k_{pdc}, k_{idc}, k_{21}, k_{31}, k_{12}, k_{22}, k_{32}, k_{14}, k_{15}, k_{24} \mathbf{I}_2, k_{34} \mathbf{I}_2, \\ & k_{ffi} \mathbf{I}_2, k_{pvi} \mathbf{I}_2, k_{ivi} \mathbf{I}_2, k_{ffv} \mathbf{I}_2, k_{pi} \mathbf{I}_2, k_{ii} \mathbf{I}_2) \hat{y} \\ = & \mathbf{K} \hat{y} \end{aligned} \quad (26)$$

where the static gain \mathbf{K} contains all the parameters to be tuned. Thereafter, the standard structure of linear fractional transformation for \mathcal{H}_∞ synthesis can be derived as shown in Fig. 6 by collapsing the MIMO-GFM converter of Fig. 4 (except for \mathbf{K}) into \mathbf{G} . As shown in Fig. 6, w and z are the defined disturbance inputs and performance outputs for the \mathcal{H}_∞ synthesis, which can be chosen according to the control objectives.

As an example, this paper considers a multi-objective problem with both active power regulation and synchronization, where w and z are chosen as

$$w = [\Delta P_{ref} \quad \Delta \omega_g]^T \quad (27)$$

$$z = [\Delta P_{ref} - \frac{1}{D_p} \Delta \omega_g - \Delta p \quad \Delta p]^T. \quad (28)$$

We use T_{ij} to represent the transfer function from w_j to z_i . In the \mathcal{H}_∞ synthesis, some weighting functions should be designed to limit the focused T_{ij} in order to obtain a favorable performance of the MIMO-GFM converter.

Specifically, T_{11} reflects the error of power tracking according to the droop characteristics. In order to have quick dynamics and small error, its weighting function is chosen as

$$W_{11} = \frac{s+8}{s+0.0008} \quad (29)$$

Similarly, T_{21} reflects the dynamics of the output active power. In order to limit the high-frequency disturbance, its weighting function is chosen as

$$W_{21} = \frac{1/80s+1}{1/8000s+1} \quad (30)$$

Last, T_{12} reflects the power regulation responding to the disturbance of the grid frequency. In order to have quick

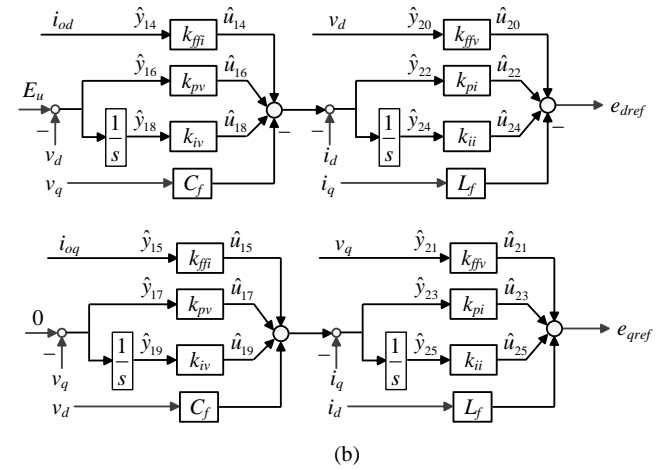
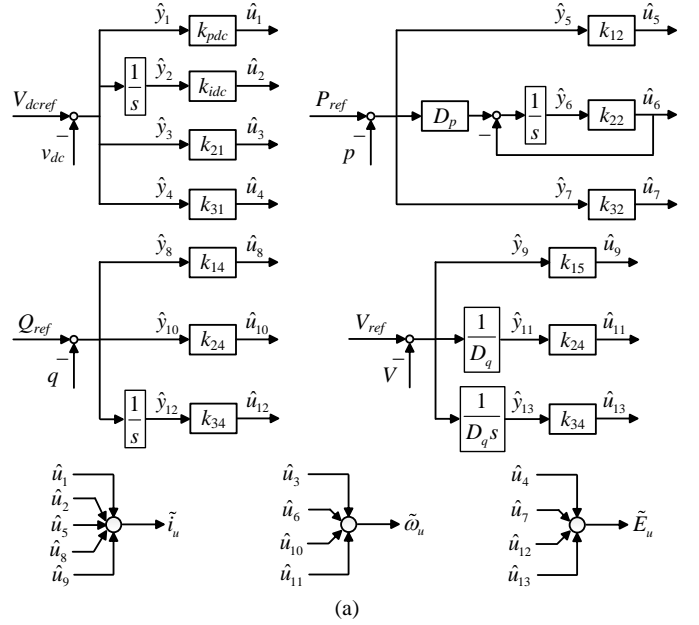


Fig. 5. Block diagram of used (a) control transfer matrix and (b) cascaded controllers.

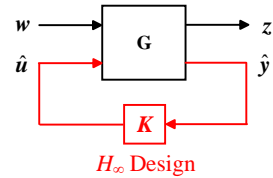


Fig. 6. Block diagram of grid-forming converter with cascaded controllers in linear fractional transformation.

dynamics and small error, its weighting function is chosen as

$$W_{12} = \frac{s+6}{100s+0.0006} \quad (31)$$

It is worth mentioning that the above equations of (27)-(31) only show an example of how to use the \mathcal{H}_∞ synthesis to tune the MIMO-GFM converter with the cascaded controllers,

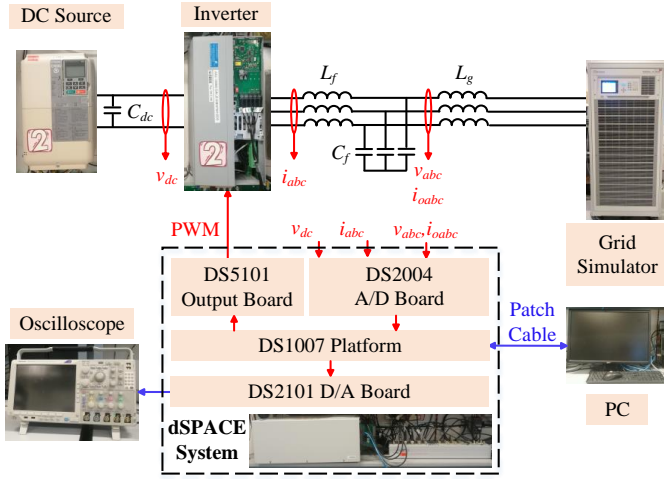


Fig. 7. Experimental configuration of MIMO-GFM converter with cascaded controllers.

TABLE I
PARAMETERS OF EXPERIMENTAL SETUPS

| Symbol | Description | Value |
|-------------|---|-------------------------------|
| ω_n | Nominal frequency | 100π rad/s |
| S_n | Nominal power | 5 kW |
| V_n | Nominal line-to-line RMS voltage | 380 V |
| f_{sw} | Switching frequency | 10 kHz |
| ω_g | Grid frequency | 100π rad/s (1 p.u.) |
| V_g | Line-to-line RMS grid voltage | 380 V (1 p.u.) |
| L_g | Line inductor | 8 mH (0.087 p.u.) |
| C_f | Filter capacitor | $5 \mu\text{F}$ (0.0454 p.u.) |
| L_f | Filter inductor | 3 mH (0.0326 p.u.) |
| C_{dc} | DC capacitor | 500 μF |
| D_p | Droop coefficient of P - f regulation | 0.01 p.u. |
| D_q | Droop coefficient of Q - V regulation | 0.05 p.u. |
| P_{ref} | Active power reference | 0.5 p.u. |
| Q_{ref} | Reactive power reference | 0 p.u. |
| V_{ref} | Voltage magnitude reference | 1 p.u. |
| V_{dcref} | DC voltage reference | 700 V |

where they can be changed according to the required performance. Meanwhile, other disturbance inputs, performance outputs, and weighting functions (e.g., for reactive power and voltage) can also be designed analogously if necessary. Thereafter, the static gain K can be obtained (e.g., by instructor *hifstruct* in Matlab) from

$$\min_K \|diag(W_{ij}(s)T_{ij}(s))\|_{\infty}. \quad (32)$$

IV. EXPERIMENTAL VALIDATION

In order to show the benefits of the \mathcal{H}_{∞} -tuned MIMO-GFM converter with cascaded controllers, the experimental results will be presented, where the configuration of the setup is shown in Fig. 7, and the key parameters are given in Table I.

TABLE II
PARAMETERS DESIGNED BY DIFFERENT METHODS

| Parameters | Traditional VSG [6], [8] | \mathcal{H}_{∞} -tuned MIMO-GFM converter |
|------------|--------------------------|--|
| k_{pi} | 0.3463 | 0.1371 |
| k_{ii} | 4.6168 | 16.7853 |
| k_{ffv} | 1 | 0.1223 |
| k_{pv} | 0.5982 | 0.7738 |
| k_{iv} | 1026.5 | 1136 |
| k_{ffi} | 0 | -0.1481 |
| k_{21} | 0 | -0.1956 |
| k_{22} | 30 | 45.1987 |
| k_{24} | 0 | -0.0458 |
| k_{31} | 0 | -0.5115 |
| k_{32} | 0 | 0.0167 |
| k_{34} | 0.1 | 0.624 |

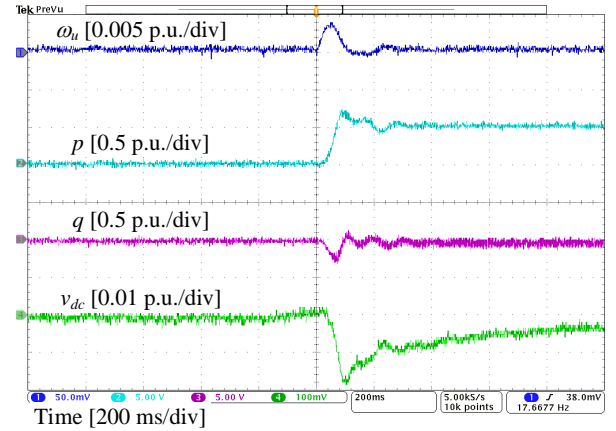


Fig. 8. Experimental results of traditional VSG when P_{ref} steps from 0.5 p.u. to 1 p.u.

A. Classic methods of parameters design

Before giving the results of the proposed \mathcal{H}_{∞} -tuned MIMO-GFM converter with cascaded controllers, the results with the classic methods for the popular virtual synchronous generator (VSG) are given as a comparison of performance in this section. The cascaded controllers are designed by the symmetrical optimum criterion and modulus optimum criterion as shown in [6]. Furthermore, the power loops are designed based on the conclusions in [8]. As the results, the derived parameters are listed in Table II. Fig. 8 and Fig. 9 show the waveform responding to P_{ref} stepping from 0.5 p.u. to 1 p.u. and ω_g decreasing from 50 Hz to 49.9 Hz, respectively. The dynamics present a stable system but with some undesired oscillations and overshoots.

B. \mathcal{H}_{∞} Synthesis of parameters design

By solving (32) with the parameters of the VSG as initial values, the parameters of the MIMO-GFM converter with

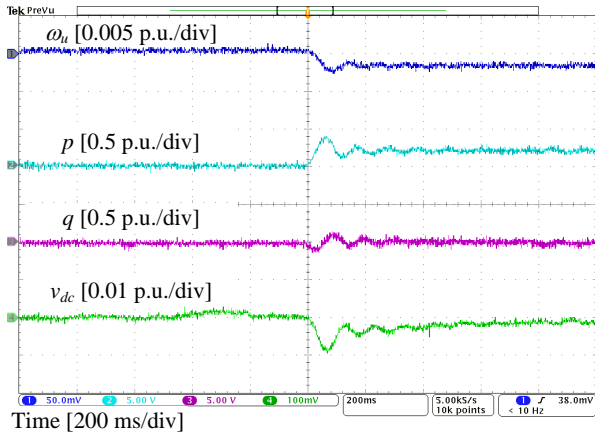


Fig. 9. Experimental results of traditional VSG when ω_g decreases from 50 Hz to 49.9 Hz

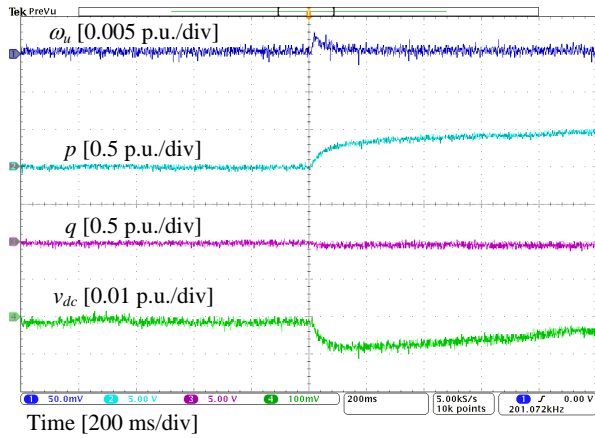


Fig. 10. Experimental results of \mathcal{H}_∞ -tuned MIMO-GFM converter when P_{ref} steps from 0.5 p.u. to 1 p.u.

cascaded controllers can be derived by \mathcal{H}_∞ Synthesis, where the results are also listed in Table II. It should be mentioned that k_{12} , k_{14} , and k_{15} are kept at 0 due to the fact that the DC control of the experimental setup is unchangeable. Fig. 10 and Fig. 11 show the waveforms of the same test cases as the traditional VSG in Section IV-A. It is observed that the MIMO-GFM converter tuned by the \mathcal{H}_∞ synthesis has much smoother dynamics with almost no overshoot. Importantly, the design of the \mathcal{H}_∞ -tuned MIMO-GFM converter is only determined by the chosen disturbance inputs w , evaluation outputs z , and weighting functions W , which are dependent on the required performance but not on assumptions of loops decoupling and bandwidths separation.

V. CONCLUSION

This paper proposes a design method of MIMO-GFM converter with cascaded controllers. A control transfer matrix based on the multivariable feedback is used to couple the DC and AC power loops. Thereafter, it shows that the parameters design can be transformed into a fix-structured \mathcal{H}_∞ optimization problem, where all the parameters including the ones

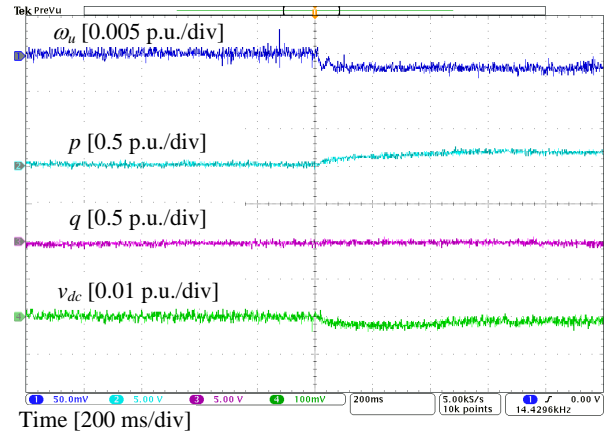


Fig. 11. Experimental results of \mathcal{H}_∞ -tuned MIMO-GFM converter when ω_g decreases from 50 Hz to 49.9 Hz

of the cascaded controllers can be tuned simultaneously. By this way, the assumptions of loops decoupling and bandwidths separation are freed and superior performances are obtained, which are illustrated by some design and experimental tests.

REFERENCES

- [1] A. Tayyebi, D. Gross, A. Anta, F. Kupzog, and F. Dörfler, "Frequency stability of synchronous machines and grid-forming power converters," *IEEE J. Emerg. Sel. Top. Power Electron.*, vol. 8, no. 2, pp. 1004–1018, Jun. 2020.
- [2] H. Wu, X. Ruan, D. Yang, X. Chen, W. Zhao, Z. Lv, and Q.-C. Zhong, "Small-signal modeling and parameters design for virtual synchronous generators," *IEEE Trans. Ind. Electron.*, vol. 63, no. 7, pp. 4292–4303, Jul. 2016.
- [3] J. Liu, Y. Miura, H. Bevrani, and T. Ise, "A unified modeling method of virtual synchronous generator for multi-operation-mode analyses," *IEEE J. Emerg. Sel. Top. Power Electron.*, vol. 9, no. 2, pp. 2394–2409, Apr. 2021.
- [4] M. Chen, D. Zhou, and F. Blaabjerg, "Active power oscillation damping based on acceleration control in paralleled virtual synchronous generators system," *IEEE Trans. Power Electron.*, vol. 36, no. 8, pp. 9501–9510, Aug. 2021.
- [5] S. D'Arco, J. A. Suul, and O. B. Fosso, "Control system tuning and stability analysis of virtual synchronous machines," in *2013 IEEE Energy Convers. Congr. Expo.*, 2013, pp. 2664–2671.
- [6] S. D'Arco, J. A. Suul, and O. B. Fosso, "Automatic tuning of cascaded controllers for power converters using eigenvalue parametric sensitivities," *IEEE Trans. Ind. Appl.*, vol. 51, no. 2, pp. 1743–1753, Mar. 2015.
- [7] S. A. Khajehoddin, M. Karimi-Ghartemani, and M. Ebrahimi, "Grid-supporting inverters with improved dynamics," *IEEE Trans. Ind. Electron.*, vol. 66, no. 5, pp. 3655–3667, May 2019.
- [8] J. Chen and T. O'Donnell, "Parameter constraints for virtual synchronous generator considering stability," *IEEE Trans. Power Syst.*, vol. 34, no. 3, pp. 2479–2481, May 2019.
- [9] C. Arghir, T. Jouini, and F. Dörfler, "Grid-forming control for power converters based on matching of synchronous machines," *Automatica*, vol. 95, pp. 273–282, Sep. 2018.
- [10] Z. Shuai, C. Shen, X. Liu, Z. Li, and Z. J. Shen, "Transient angle stability of virtual synchronous generators using lyapunov's direct method," *IEEE Trans. Smart Grid*, vol. 10, no. 4, pp. 4648–4661, Jul. 2019.
- [11] A. Tayyebi, A. Anta, and F. Dörfler, "Hybrid angle control and almost global stability of grid-forming power converters," *arXiv preprint arXiv:2008.07661*, 2020.
- [12] X. Xiong, C. Wu, and F. Blaabjerg, "An improved synchronization stability method of virtual synchronous generators based on frequency feedforward on reactive power control loop," *IEEE Trans. Power Electron.*, vol. 36, no. 8, pp. 9136–9148, Aug. 2021.

- [13] B. B. Johnson, B. R. Lundstrom, S. Salapaka, and M. Salapaka, "Optimal structures for voltage controllers in inverters," 2018, pp. 1–6.
- [14] A. Fathi, Q. Shafiee, and H. Bevrani, "Robust frequency control of microgrids using an extended virtual synchronous generator," *IEEE Trans. Power Syst.*, vol. 33, no. 6, pp. 6289–6297, Nov. 2018.
- [15] C. Kammer, S. D'Arco, A. G. Endegnanew, and A. Karimi, "Convex optimization-based control design for parallel grid-connected inverters," *IEEE Trans. Power Electron.*, vol. 34, no. 7, pp. 6048–6061, Jul. 2019.
- [16] E. Sánchez-Sánchez, D. Groß, E. Prieto-Araujo, F. Dörfler, and O. Gomis-Bellmunt, "Optimal multivariable MMC energy-based control for DC voltage regulation in hvdc applications," *IEEE Trans. Power Deliv.*, vol. 35, no. 2, pp. 999–1009, Apr. 2020.
- [17] S. Dadjo Tavakoli, S. Fekriasl, E. Prieto-Araujo, J. Beerten, and O. Gomis-Bellmunt, "Optimal H infinity control design for MMC-based HVDC links," *IEEE Trans. Power Deliv.*, Early Access 2021.
- [18] L. Huang, H. Xin, and F. Dörfler, " \mathcal{H}_∞ -control of grid-connected converters: Design, objectives and decentralized stability certificates," *IEEE Trans. Smart Grid*, vol. 11, no. 5, pp. 3805–3816, Sep. 2020.
- [19] M. Chen, D. Zhou, A. Tayyebi, E. Prieto-Araujo, F. Dörfler, and F. Blaabjerg, "Generalized multivariable grid-forming control design for power converters," *arXiv preprint arXiv:2109.06982*, 2021.